Available online at www.sciencedirect.com
SCIENCE DIRECT®
Journal of Magnetism and Magnetic Materials 270 (2004) 22–31
www.elsevier.com/locate/jmmm

An analytical model for ultrathin films with spatially varying magnetic anisotropies

F. Porrati*, W. Wulfhekel, J. Kirschner

Max-Planck-Institut für Mikrostrukturphysik, Weinberg 2, D-06120 Halle, Germany

Received 25 October 2002

Abstract

The continuum theory of micromagnetism is used to study ultrathin films with magnetic anisotropy varying laterally on the nanometer scale. A series of infinitely long stripes with alternating in- and out-of-plane uniaxial anisotropy is considered as a model for patterned ferromagnetic films. The analytical solution based on an effective anisotropy description of the dipolar energy is given as a function of the material parameters (exchange and anisotropy constants) and the width of the stripes. States of uniform and non-uniform magnetization are obtained. For film of finite thickness the exact value of the dipolar energy is calculated numerically and the numerical solution is compared with the analytical one. We find that the correction to the dipolar energy is negligible for nickel, while for cobalt and iron it has to be considered as a function of the anisotropies, the width of the stripes and the thickness of the film.

PACS: 75.70.Ak; 75.30.Gw

Keywords: Magnetic anisotropy; Micromagnetism; Ultrathin films

1. Introduction

Modern nanofabrication techniques allow the design of new magnetic devices [1]. Nanopatterning can be achieved by means of ion irradiation [2,3], self-organization [4,5], growth on vicinal single-crystal substrates [6,7] and lithography. This last technique is particularly suitable to obtain model samples well-ordered magnetically and well-defined morphologically in reduced dimensions. Driven by the large number of potential applications, in the last decade a lot of effort has been put in the study of multi-layer devices. Only recently the interest for lateral magnetic nanostructures [5,7,8] has increased because of the progress in fabrication. The lateral investigation below ~ 100 nm is possible by means of magnetic force microscopy [9] and scanning electron microscopy with spin polarization analysis [10]. Besides, recent advances in scanning tunneling microscopy and spectroscopy allow to image magnetic structures with nanometer resolution by using ferromagnetic tips [11,12].

With the advent of nanotechnology the task of micromagnetics is to connect the magnetic properties of the material with the morphological

*Corresponding author. Physikalisches Institut Dnne Schichten, Frankfurt University, Robert-Mayer Str. 2-4, 60054 Frankfurt am Main, Germany. Tel.: +496979822132; fax: +496979822348.

E-mail address: porrati@physik.uni-frankfurt.de (F. Porrati).

0304-8853/$ - see front matter © 2003 Elsevier B.V. All rights reserved.
doi:10.1016/S0304-8853(03)00658-9

structure obtained by fabrication. The task is fundamental because on the nanometer scale the structure of the material competes with the micromagnetic characteristic length. At nanoscale, new magnetic phenomena are expected, as recently theoretically examined [13] and experimentally found [14].

In thin films the breaking of symmetry at the surface generates an anisotropy that can favor either an in-plane or an out-of-plane magnetization [15]. The direction of the easy axis may change if a new layer is added to cap the system [16–18]. The capping layer can cover the system entirely or partially. In the last case the surface anisotropy varies locally and, as a consequence, the direction of the magnetization may be a function of the position [19]. These systems can be modeled analytically by means of a series of stripes with alternating in- and out-of-plane uniaxial anisotropies. In this work, the analytical solution of the problem, exact in the limit of infinitely thin films, is given as a function of the system parameters. In this case the dipolar energy is treated as a local demagnetizing energy and is part of the anisotropy energy. For films of finite thickness the exact solution is obtained numerically by computer simulation[1] and is compared with the approximated analytical one.

2. The model

The geometry of the problem is shown in Fig. 1. The unit cell consists of two stripes infinitely long in the y direction of width L_1 and L_2 with easy axis out-of-plane and in-plane, respectively. The geometry repeats along the x direction, so that the magnetization results symmetric with respect to the center of each stripe.

The magnetization vector $\mathbf{M}$ is uniform in the vertical direction since the thickness of the slab is smaller than the magnetic characteristic length [22]. Furthermore $\mathbf{M}$ is assumed to lie in the yz plane and to vary only along x, i.e., $\mathbf{M}=\mathbf{M}(x)$. Therefore the divergence of the magnetization is zero and only the surface charges contribute to the magnetostatic energy.

[1] The simulations are performed with LLG *Micromagnetic Simulator*^{TM} by M. Scheinfein.

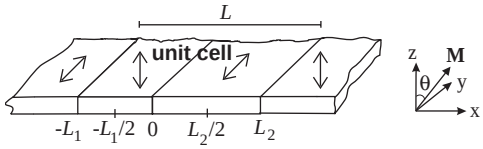

Fig. 1. Unit cell for a system with alternating uniaxial anisotropies. The easy axis of the anisotropy is out-of-plane in the stripe of width L_1 and in-plane in the stripe of width L_2.

2.1. Magnetization profiles

The total energy per unit area of the unit cell is given by [21,22]:

$$G(L_1,L_2)=\int_{-L1}^{0} f_1(x)\,\mathrm{d}x+\int_{0}^{L_2} f_2(x)\,\mathrm{d}x, \tag{1}$$

where the energy densities f_1 and f_2 are given by

$$f_1(x)=A_1\left(\frac{\mathrm{d}\theta}{\mathrm{d}x}\right)^2+k_{\mathrm{sh}}\cos^2\theta+k_1\sin^2\theta, \quad -L_1\leqslant x\leqslant 0, \tag{2}$$

$$f_2(x)=A_2\left(\frac{\mathrm{d}\theta}{\mathrm{d}x}\right)^2+k_{\mathrm{sh}}\cos^2\theta+k_2\sin^2\theta, \quad 0\leqslant x\leqslant L_2, \tag{3}$$

k_1 and k_2 being the magneto-crystalline anisotropy constants and $\theta(x)$ the angle between $\mathbf{M}(x)$ and the normal to the film. The constant $k_{\mathrm{sh}}=2\pi M_{\mathrm{s}}^2$ gives the value of the shape anisotropy (or magnetostatic energy) for an infinite film out-of-plane uniform magnetized. The first term of Eqs. (2) and (3) is the exchange energy density, A_1 and A_2 being the exchange stiffness constants. The remaining part is the sum of the shape and the magneto-crystalline anisotropy energies. Since these quantities have the same angular dependence, they can be written by using the effective anistropies $k_1^{\mathrm{eff}}=k_1-k_{\mathrm{sh}}>0$, that favors an out-of-plane magnetization and $k_2^{\mathrm{eff}}=k_2-k_{\mathrm{sh}}<0$, that favors an in-plane magnetization. In this formulation only the local demagnetizing energy is considered. Minimizing Eq. (1) we obtain $\theta(x)$. By applying

variational calculus [23] it follows:

$$\left(\frac{d\theta}{dx}\right)^2 = \frac{\sin^2\theta}{\lambda_1^2} + c_1, \quad -L_1 \leqslant x \leqslant 0, \tag{4}$$

$$\left(\frac{d\theta}{dx}\right)^2 = -\frac{\sin^2\theta}{\lambda_2^2} + c_2, \quad 0 \leqslant x \leqslant L_2 \tag{5}$$

with $\lambda_1 = \sqrt{A_1/k_1^{\text{eff}}}$ and $\lambda_2 = \sqrt{-A_2/k_2^{\text{eff}}}$ positive quantities, c_1 and c_2 constants to be determined. Since the structure is periodic along the x direction, the derivative of θ at the center of the stripes must be zero, i.e., $\lim_{x\to -L_1/2}(d\theta/dx) = 0$ and $\lim_{x\to L_2/2}(d\theta/dx) = 0$. As a consequence Eqs. (4) and (5) become

$$\left(\frac{d\theta}{dx}\right)^2 = \frac{\sin^2\theta - \sin^2\theta(-L_1/2)}{\lambda_1^2}, \quad -L_1 \leqslant x \leqslant 0, \tag{6}$$

$$\left(\frac{d\theta}{dx}\right)^2 = \frac{\sin^2\theta(L_2/2) - \sin^2\theta}{\lambda_2^2}, \quad 0 \leqslant x \leqslant L_2. \tag{7}$$

Taking the square root and integrating along the x direction, Eq. (7) results:

$$\int_{\theta(0)}^{\theta(x)} \frac{d\theta}{\sqrt{1 - m\sin^2\theta}} = \frac{x}{\lambda_2\sqrt{m}}, \tag{8}$$

where $\theta(0)$, the angle of the magnetization at the border between two stripes, is an unknown parameter and $m = (\sin^2\theta(L_2/2))^{-1}$. Since Eq. (9) is the difference between elliptical integrals of the first kind [24], we obtain

$$F(\theta(x)|m) - F(\theta(0)|m) = \frac{x}{\lambda_2\sqrt{m}}. \tag{9}$$

By means of the properties of the elliptical integrals Eq. (9) transforms into

$$F\left(a\sin\left(\frac{\sin\theta(x)}{\sin\theta(L_2/2)}\right)|\sin^2\theta(L_2/2)\right) - F\left(a\sin\left(\frac{\sin\theta(0)}{\sin\theta(L_2/2)}\right)|\sin^2\theta(L_2/2)\right) = \frac{x}{\lambda_2}. \tag{10}$$

Eq. (10) is valid for $0 \leqslant x \leqslant L_2$ and is symmetric with respect to the center of the stripe, i.e. $x = L_2/2$. In the same way from Eq. (6) we obtain

$$F\left(a\sin\left(\frac{\cos\theta(x)}{\cos\theta(-L_1/2)}\right)|\cos^2\theta(-L_1/2)\right) - F\left(a\sin\left(\frac{\cos\theta(0)}{\cos\theta(-L_1/2)}\right)|\cos^2\theta(-L_1/2)\right) = -\frac{x}{\lambda_1} \tag{11}$$

valid for $-L_1 \leqslant x \leqslant 0$. To extract $\theta(x)$ from Eqs. (10) and (11) we use the Weierstrass–Erdmann law [25]:

$$A_1\left(\frac{d\theta}{dx}\right)_{x=-0} = A_2\left(\frac{d\theta}{dx}\right)_{x=+0}. \tag{12}$$

By inserting Eqs. (6) and (7) in Eq. (12) we obtain

$$\cos^2\theta(-L_1/2) = \cos^2\theta(0)(1+\xi) - \xi\cos^2\theta(L_2/2) \tag{13}$$

with $\xi = k_2^{\text{eff}}/k_1^{\text{eff}}$. Eqs. (10), (11) and (13) constitute a system of equations from which $\theta(x)$ can be extracted.

As an example let us consider a system with unit cell L such that $L_1/L_2 = 2/3$. The exchange stiffness and the absolute values of the effective anisotropy are the same in the two stripes, i.e., $A_1 = A_2 = 10^{-6}$ erg/cm and $k_1^{\text{eff}} = -k_2^{\text{eff}} = 1\times 10^7$ erg/cm^3. The resulting magnetization profile is plotted in Fig. 2 for a unit cell $L = 15$ nm. Since $L_1 \neq L_2$ the angular dependence of the magnetization is asymmetric with respect to the center of the unit cell and the angle at the border between two neighbour stripes is $\theta(0) \neq 45°$. In this example $\theta(0)$

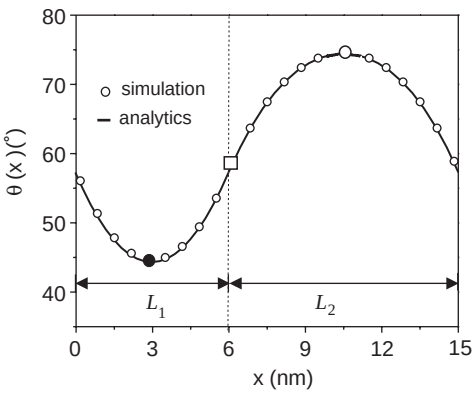

Fig. 2. Magnetization profile across two neighbor stripes. The numerical solution agrees with the analytical one in the limit of infinitely thin films (see text).

is bigger than 45° because $L_2 > L_1$. In Fig. 2 we compare the analytical solution with the numerical one obtained in the limit of infinitely thin films. The perfect agreement between the two curves shows that the numerical solution is correct. In Section 2.3 we will compare the two curves in the case of films of finite thickness where the numerical solution is exact and the analytical one is an approximation. It is worth noting that for infinitely thin films the dipolar interaction does not play any role in the formation of the magnetic microstructure that is rather due to the balance between the exchange and the effective anisotropies. Moreover, the stability of the analytical solution is guaranteed by the non-homogeneity of the anisotropy. In fact, Brown and Shtrikman showed that in a one-dimensional homogeneous ferromagnet all the solutions in which the magnetization is non-uniform are unstable [26,27].

The problem of the determination of the geometrical size under which a ferromagnet is uniformly magnetized was solved by Brown in the case of fine particles with uniaxial anisotropy [28]. Brown rigorously proved that a sphere is uniformly magnetized below a certain critical radius determined by the exchange and the anisotropy constants. In the case of a thin film, Thiaville and Fert showed that for transition metals the magnetization is homogeneous in the vertical direction and never modulated [20]. In this case, in spite of the presence of the surface anisotropy the exchange stiffness constant is considered to be strong enough to keep all the magnetic moments aligned. This result allowed us to reduce our analysis to one- dimension, i.e., the magnetization is considered not to vary across the film thickness. The first author who addressed the problem for ultrathin films with laterally varying magnetic anisotropies was Elmers, who calculated the transition point to the uniform configuration using the Jacobi criterion [21]. This result defines the regions of uniform and non-uniform magnetization, but does not clarify how the transition takes place. By means of Eqs. (10), (11) and (13) it is possible to study the magnetization profile as a function of the system's parameters. In particular the transition between non-uniform and uniform magnetization can be studied by shrinking the width of the unit cell. In order to study the transition we have determined the direction of the magnetization at the center of the two stripes, i.e. $\theta(-L_1/2)$ and $\theta(L_2/2)$, and at the border between them, i.e., $\theta(0)$. The result of this calculation is shown in Fig. 3 (top right) where the values obtained numerically and analytically are compared showing an excellent agreement.

In Fig. 3 we have plotted two magnetization profiles obtained for large and small values of the width of the unit cell, i.e., $L \gg \lambda$ and $L \leqslant \lambda$. In the first case (see bottom left of Fig. 3) the unit cell is so wide ($L = 45$ nm) that the magnetization is almost parallel to the easy axis at the center of the stripes: $\theta(L_1/2) \approx 5°$ and $\theta(L_2/2) \approx 90°$. Shrinking the width of the system the relative importance of the exchange energy increases and therefore the amplitude of the modulation of the magnetization reduces, until the magnetization becomes uniform ($L \leqslant 10$ nm) (bottom right of Fig. 3). Since $L_2 > L_1$ the angle $\theta(0)$ tends to rotate in-plane with the reduction of L. $\theta(-L_1/2)$ behaves similarly. The behavior of the two curves with respect to the width of the unit cell is monotonic, while $\theta(L_2/2)$ has a minimum around $L = 15$ nm. The existence of the minimum shows that there are two factors determining the direction of the magnetization. On the one hand the exchange energy that tries to reduce $\theta(L_2/2)$ in order to minimize the amplitude of the modulation. On the other hand the geometry of the system that favors the rotation of the magnetization in-plane and thus the increase of $\theta(L_2/2)$. Finally, a continuous transition between states of non-uniform and uniform magnetization is obtained upon shrinking the width of the unit cell.

2.2. The magnetic energy

The exchange energy per unit volume is given by:

$$f_{\mathrm{ex}} = \frac{2}{L} A_1 \int_{-L_1/2}^{0} \left(\frac{\mathrm{d}\theta}{\mathrm{d}x}\right)^2 \mathrm{d}x + \frac{2}{L} A_2 \int_{0}^{L2/2} \left(\frac{\mathrm{d}\theta}{\mathrm{d}x}\right)^2 \mathrm{d}x. \tag{14}$$

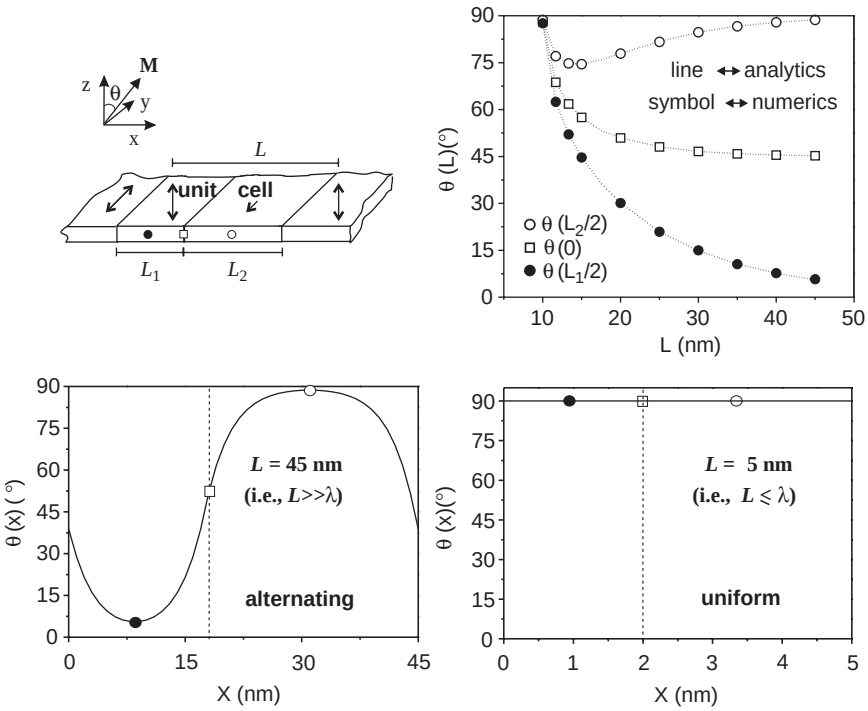

Fig. 3. In the top panel some reference angle, see sketch, are plotted as a function of L, width of the unit cell. By changing L the magnetization profile results either alternating (bottom left) or uniform (bottom right).

By integration, see appendix, Eq. (14) transforms into

$$f_{\mathrm{ex}} = \frac{2A_1}{\lambda_1 L}\left(\Delta E(\phi_1|m_1) - (1-m_1)\frac{L_1}{2\lambda_1}\right) + \frac{2A_2}{\lambda_2 L}\left(\Delta E(\phi_2|m_2) - (1-m_2)\frac{L_2}{2\lambda_2}\right) \qquad (15)$$

with $\Delta E(\phi_1|m_1) = E(\phi(-L_1/2)|m_1) - E(\phi(0)|m_1)$, $\Delta E(\phi_2|m_2) = E(\phi(L_2/2)|m_2) - E(\phi(0)|m_2)$, $m_1 = \cos^2\theta(-L_1/2)$ and $m_2 = \sin^2\theta(L_2/2)$. $E(\phi|m)$ is the elliptical integral of the second kind. A compact form of Eq. (15) is obtained when $A_1 = A_2 = A$, $L_1 = L_2 = L/2$ and $\lambda_1 = \lambda_2 = \lambda$:

$$f_{\mathrm{ex}} = \frac{4A}{\lambda L}\left(E(\phi(L/4)|m) - E(\phi(0)|m) - (1-m)\frac{L}{4\lambda}\right). \qquad (16)$$

In the derivation of Eq. (16) also the condition of symmetry $\theta(-L_1/2) + \theta(L_2/2) = \pi/2$, that leads to $m_1 = m_2 = m$ and $\phi(-L_1/2) = \phi(L_2/2) = \phi(L/4)$, has been used.

In Fig. 4 the exchange energy density is plotted as a function of L, width of the unit cell. The system considered is Ni on Cu(0 0 1) partially covered by H_2. The film of Ni on Cu(0 0 1) with a thickness below 10 monolayers is magnetized in-plane; adsorption of H_2 changes the surface anisotropy so that an out-of-plane magnetization becomes favorable [29]. This system is a good candidate for experimental studies for films with alternating anisotropies. In fact, by e-beam irradiation it is possible to partially remove H_2, until a scale of $\sim$10 nm, in order to prepare films with spatially varying magnetic anisotropies. The sum of the interface and the surface anisotropy is $k_{\mathrm{s}+i,\mathrm{Ni}} = -0.611\,\mathrm{erg/cm^2}$ for Ni on Cu(0 0 1) and $k_{\mathrm{s+i},\mathrm{H_2}} = -0.396\,\mathrm{erg/cm^2}$ when H_2 is adsorbed [29]. Considering that the value of the volume anisotropy is $k_{\mathrm{v}} = 0.439 \times 10^7\,\mathrm{erg/cm^3}$ and the shape anisotropy is $k_{\mathrm{sh}} = 1.098 \times 10^6\,\mathrm{erg/cm^3}$, for a thickness of 9 ML we have $k_{H_2}^{\mathrm{eff}} = -k_{\mathrm{Ni}}^{\mathrm{eff}} =$

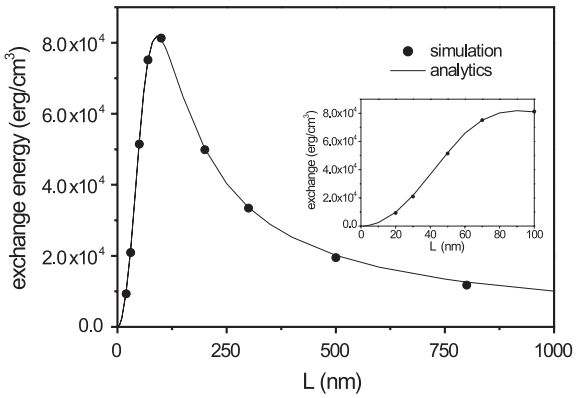

Fig. 4. Exchange energy density vs. L, width of the unit cell. The curve refers to the system H_2/Ni/Cu(0 0 1) (see text). The dots are the result of the simulation, where the dipolar interaction is exactly considered. The line plots Eq. (16).

0.702×10^6 erg/cm^3. By means of Eq. (16) we can study the exchange energy as a function of the width of the unit cell. The angle between neighbor magnetic moments increases with L. As a consequence also the exchange energy increases since it is proportional to the square of the derivative of the angle to the normal, i.e., $f_{ex} \propto (d\theta/dx)^2$. If L is wide enough so that the magnetic structure is virtually free of geometrical constrictions, any further increase of the width of the unit cell does not increase the exchange energy. Therefore, after the maximum, the exchange energy density decreases with power law L^{-1}. The perfect agreement between analytical and numerical solution shows that the exchange energy is correctly predicted for H_2/Ni/Cu(0 0 1) if the demagnetizing energy is treated as an anisotropy term.

In the anisotropy-type description the sum of the magnetostatic energy and of the anisotropy energy is given by

$$f_{ms} + f_{an} = k_{sh} + \frac{2}{L} k_1^{eff} \int_{-L_1/2}^{0} \sin^2\theta(x)\,dx + \frac{2}{L} k_2^{eff} \int_{0}^{L_2/2} \sin^2\theta(x)\,dx. \quad (17)$$

After integration, see Appendix, Eq. (17) becomes

$$f_{ms} + f_{an} = k_{sh} + \frac{2k_1^{eff}\lambda_1}{L}\Delta E(\phi_1|m_1) - \frac{2k_2^{eff}\lambda_2}{L}\Delta E(\phi_2|m_2) + \frac{L_2 k_2^{eff}}{L}. \quad (18)$$

With the same conditions used to obtain Eq. (16), Eq. (18) transforms into

$$f_{ms} + f_{an} = \frac{k_{sh} + k_2}{2} + \frac{4k_1^{eff}\lambda_1}{L}\left(E\left(\phi\left(\frac{L}{4}\right)|m\right) - E(\phi(0)|m)\right). \quad (19)$$

Eq. (19) is plotted in Fig. 5 as a function of L in the case of Ni on Cu(0 0 1) partially covered by H_2. The second term Eq. (19) is a positive number that reduces with increasing L. In the limit of large unit cell the magnetization in successive stripes alternates between in-plane and out-of-plane directions. Therefore, since $L_1 = L_2 = L/2$, the magnetostatic energy density is half of the value obtained for a film magnetized uniformly out-of-plane, i.e., $f_{ms} = k_{sh}/2$ because the magnetic surface charges are only present in the stripes with out-of-plane anisotropy. Similarly the anisotropy energy density due to the contribution inside the stripes of Ni, which are in-plane magnetized, is $f_{an} = k_{Ni}/2 = k_2/2$. In the limit of vanishing width

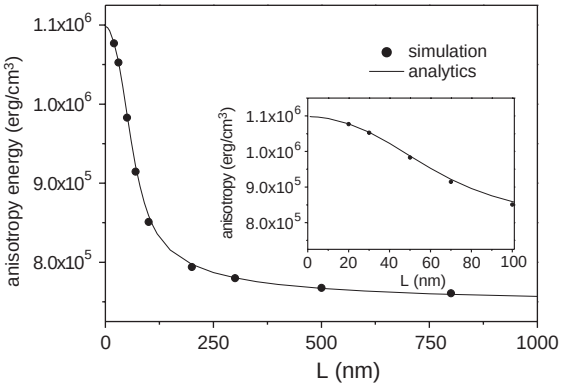

Fig. 5. Effective anisotropy energy vs. L, width of the unit cell. The maximum value is obtained for $L \to 0$ when the magnetization is uniform at 45° with respect to the normal. The minimum is reached for large width of the unit cell when the magnetization alternates from in-plane to out-of-plane in successive stripes.

of the unit cell, the magnetization is uniform at 45° with respect to the normal. As a consequence the integrand function contained in Eq. (17) is constant and the integration is straightforward. Considered that $k_1^{\text{eff}} = -k_2^{\text{eff}}$, it follows $f_{\text{ms}} + f_{\text{an}} = k_{\text{sh}}$. In this way we find that in the limit of small unit cell, i.e., for $L \to 0$, the effective anisotropy energy is equal to the magnetostatic energy of a film uniformly magnetized out-of-plane. It is interesting to notice that the second derivative of the anisotropy energy changes sign for $L \approx 50$ nm. The same behavior is found in the plot of the exchange energy, see inset of Fig. 4. The existence of the point of inflection is the result of two competing factors that contribute to the variation of the energy as a function of L. For $L < 50$ nm the dependence of the fine structure, represented by the elliptical integrals, dominates the energy variation; for $L > 50$ nm the geometrical scale factor $1/L$ becomes dominant since the magnetization is almost free from geometric constrain, i.e., the contribution of the elliptical integral is constant with L. The good agreement of the value of the effective anisotropy, together with the exchange energy, obtained analytically and numerically shows that the anisotropy-type description is correct for any width of the unit cell.

The total energy is a function of L and is given by the sum of Eqs. (15) and (18). The gain in energy due to the modulation of the magnetization is given by

$$\Delta f_t(L) = f_t^{\text{unif}} - f_t^{\text{mod}}(L) \tag{20}$$

being f_t^{unif} a state of uniform magnetization function of the effective anisotropies. If $L_1 k_1^{\text{eff}} > L_2 k_2^{\text{eff}}$ the out-of-plane anisotropy dominates and $f_t^{\text{unif}} = k_{\text{sh}}$. If $L_1 k_1^{\text{eff}} < L_2 k_2^{\text{eff}}$ the in-plane anisotropy dominates and $f_t^{\text{unif}} = k_1 + k_2$. If the effective anisotropies balance, i.e., $L_1 k_1^{\text{eff}} = L_2 k_2^{\text{eff}}$, the magnetization tilts at 45° for $L \to 0$ and $f_t^{\text{unif}} = k_{\text{sh}}$, as seen above. In this case Eq. (20) becomes

$$\Delta f_t(L) = \left(\frac{1}{2} - m\right) k_1^{\text{eff}} - \frac{8}{L} k_1^{\text{eff}} \lambda \left(E\left(\phi\left(\frac{L}{4}\right)|m\right) - E(\phi(0)|m)\right). \tag{21}$$

Eq. (21) as a function of L is plotted in Fig. 6 in the case of Ni on Cu(0 0 1) partially covered by H_2.

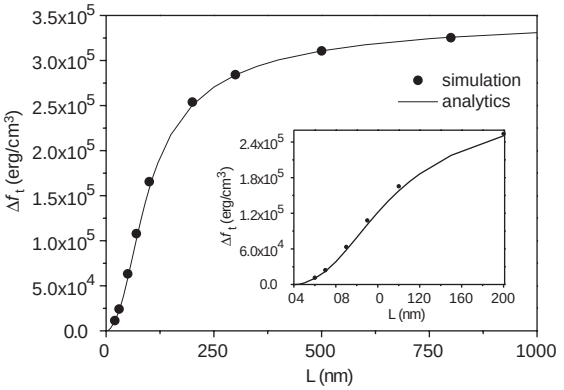

Fig. 6. Energy gain due to the modulation of the anisotropy vs. L, width of the unit cell.

Comparison between Figs. 4 and 5 shows that the anisotropy energy is at least one order of magnitude larger than the exchange energy and therefore dominates the behavior of $\Delta f_t(L)$. Note that in the limit of small stripes, i.e., $L \leqslant \lambda$, the magnetization slightly oscillates around 45° giving rise to a canted state represented macroscopically by a fourth-order anisotropy term [19,30].

The scaling properties of the system are briefly addressed in the following. Let us define two magnetization profiles as equivalent if their shape is the same after scaling of the width of the unit cell, i.e., $L_1/L_2 = \text{const}$. The scale invariance of the magnetization profiles is obtained with the analysis of Eqs. (10) and (11). These equations are invariant for $L_1/\lambda_1 = a$ and $L_2/\lambda_2 = b$, where a and b are constants. In particular if the effective anisotropies balance the scaling variable is L/λ. In this case also the reduced energy $\Delta f_t(L)/k_{\text{eff}}$ is invariant, see Eq. (21).

2.3. The role of the dipolar interaction

The alternating anisotropies produce a modulation of the magnetization and thus of magnetic surface charge. As a consequence the stray field is non-uniform and, if the thickness of the film is finite, a torque is generated in the stripe with in-plane anisotropy (see Fig. 7). This torque can modify the profiles calculated in the effective anisotropy approximation. The comparison between anisotropy-type description (analytics) and

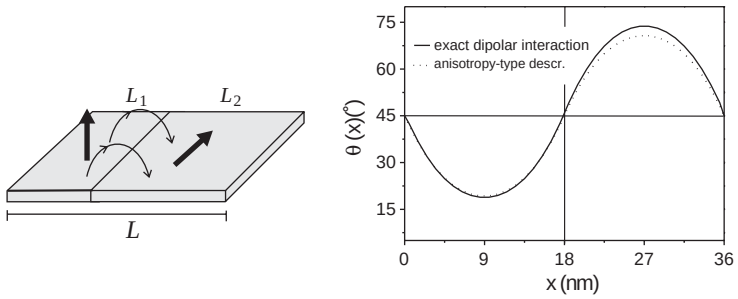

Fig. 7. Comparison between the magnetization profiles obtained in the anisotropy-type approximation (dotted line) and in the fully dipolar interaction description (full line).

fully dipolar description (simulation) shows that the correction to the energy due to the dipolar interaction for Ni/Cu(0 0 1) partially covered by H_2 is negligible. The generality of this result is not a priori guaranteed. In fact, the effect of the stray field is expected to be stronger than in H_2/Ni/Cu(0 0 1) in systems of higher thickness or with higher value of the magnetic moments. In Fig. 7 is plotted the magnetizazion profile for a film of 4ML of Co/Pd(1 1 1) partially covered by Pd. The width of the unit cell is $L = 36$ nm and the effective anisotropies $k_{\mathrm{Pd}}^{\mathrm{eff}} = -k_{\mathrm{Co}}^{\mathrm{eff}} = 0.48 \times 10^7\ \mathrm{erg/cm^3}$. The effect of the torque shows up in a rotation of the magnetic moments in the in-plane stripe and, as a consequence, in a decrease of the magnetostatic energy.

The rotation is a function of the value of the effective anisotropy, the width of the unit cell and the thickness of the film. The error that we make by using the analytical solution to describe films of finite thickness is plotted in Fig. 8. In Fig. 8a the variation of the magnetostatic energy, i.e., $\Delta f_{\mathrm{ms}}/f_{\mathrm{ms}}$, is plotted versus the effective anisotropy for a film of iron of thickness $t = 0.6$ nm and unit cell of width $L \approx 40$ nm. The plot, obtained with the scaling procedure introduced above, shows that the softer the material is, the stronger is the effect of the dipolar interaction. For systems with $k_{\mathrm{eff}} > 4 \times 10^6\ \mathrm{erg/cm^3}$ the error is smaller than 3%. In Fig. 8b the error is plotted versus the width of the unit cell for the same system with an effective anisotropy $k_{\mathrm{eff}} = 4 \times 10^6\ \mathrm{erg/cm^3}$ (stars). The effect of the stray field is negligible ($\Delta f_{\mathrm{ms}}/f_{\mathrm{ms}} < 1\%$) for $L < 10$ nm, where the exchange interaction is strong enough to keep the magnetic moment almost parallel. If the unit cell of the system increases the magnetic moments follow the alternating anisotropy and the stray field induces their rotation. The maximum variation is obtained for $L \approx 40$ nm. For $L > 40$ nm the effect of the rotation decays as $\sim -1/L$, like the magnetic potential. The value of Δf_{ms} is a function of the saturation magnetization M_{s}. Among the 3d ferromagnetic transition metals the variation is maximum for iron ($M_{\mathrm{s}} = 1714\ \mathrm{emu/cm^3}$) and minimum for nickel ($M_{\mathrm{s}} = 470\ \mathrm{emu/cm^3}$). The effect of the stray field is negligible for $L < 10$ nm and $L > 80$ nm for each material and in the whole range of widths of the unit cell in the case of nickel. Finally, the stray field is a function of the thickness of the film [31] and its effect may be evaluated for a fixed width of the unit cell ($L = 40$ nm) and the effective anisotropy ($k_{\mathrm{eff}} = 4 \times 10^6\ \mathrm{erg/cm^3}$), see Fig. 8c. The plot shows that the variation of the magnetostatic energy grows linearly with the thickness and increases with M_{s}. It is worth noting that in general the magnetic anisotropy is not constant but is a function of the thickness of the film. As a consequence in real systems the thickness dependence of the stray field will be in general not linear.

3. Summary

In this work, a periodic system of stripes with alternating anisotropies has been studied by means of micromagnetics. The magnetization profiles and the energies have been analytically calculated as a function of the system's parameters by considering the dipolar energy as a local demagnetizing energy. The magnetization profiles scale linearly with the ratio L/λ between the width of the unit cell and the

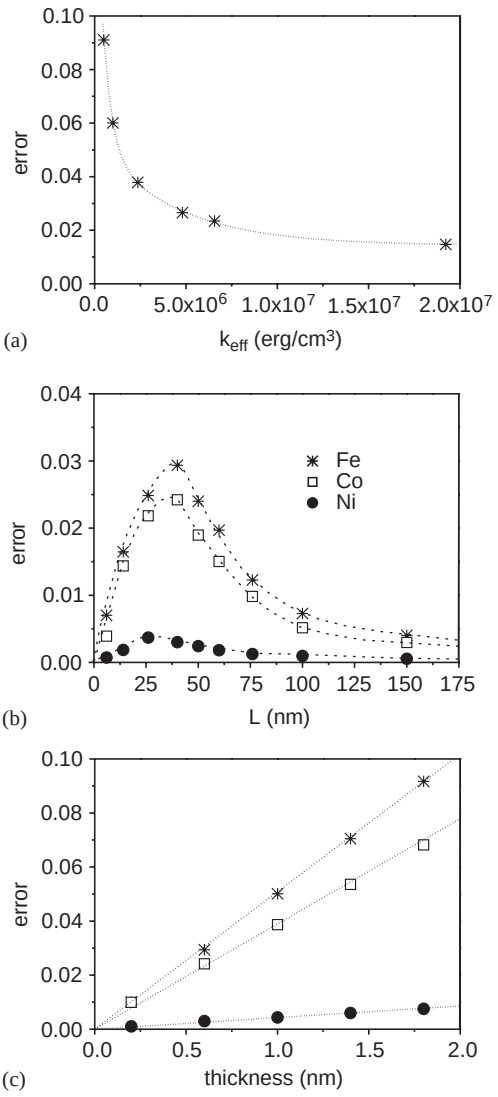

Fig. 8. Error made by considering the analytical solution as valid for films of finite thickness. The error is a function of the effective anisotropy (a), the width of the unit cell (b), the thickness of the slab (c) and of the saturation magnetization (b,c). The same exchange stiffness constant $A = 1.55 \times 10^{-6}$ erg/cm^3 has been used in the calculations.

magnetic characteristic length. A transition between non-uniform and uniform magnetization occurs by shrinking the width of the unit cell of the system. Finally, for films of finite thickness the approximated analytical solution is compared with the numerical one that contains the exact value of the dipolar interaction. The comparison shows that the effect of the stray field is always negligible for nickel. In the case of cobalt and iron the effect has to be considered as a function of the anisotropy, the scale and the thickness of the system. In conclusion, in the limits indicated, we have found that the analytical solution is of high accuracy and numerical modeling is not necessary. Therefore the analytical solution can be used to determine the anisotropy constants by fitting experimental magnetization profiles. For applications, ultrathin films with spatially varying magnetic anisotropies might be used as high storage magnetic media and as magnetic field sensors.

Acknowledgements

The authors acknowledge H.P. Oepen, G. Steierl and R. Hertel for fruitful discussions.

Appendix A

A.1. Derivation of Eq. (15)

The following integrals contained in Eq. (14) have to be solved

$$I_1 = \int_{-L_1/2}^{0} \left(\frac{\mathrm{d}\theta(x)}{\mathrm{d}x}\right)^2 \mathrm{d}x,$$

$$I_2 = \int_{0}^{L_2/2} \left(\frac{\mathrm{d}\theta(x)}{\mathrm{d}x}\right)^2 \mathrm{d}x. \tag{A.1}$$

With the change of variable $\theta(x) = \arcsin(\sqrt{m_2}\sin\phi(x))$, where $m_2 = \sin^2\theta(L_2/2)$, we calculate the integrand function of I_2:

$$\frac{\mathrm{d}\theta(x)}{\mathrm{d}x} = \frac{\sqrt{m_2}}{\lambda_2}\,\mathrm{cn}(F(\phi(x)|m_2)). \tag{A.2}$$

Substituting we obtain

$$I_2 = \frac{m_2}{\lambda_2}\int_0^{L_2/2} \mathrm{cn}^2 z\,\mathrm{d}z, \tag{A.3}$$

where $z = x/\lambda_2 + F(\phi(0)|m_2)$. Using the properties of the elliptical integral it follows

$$I_2 = \frac{E(\phi(L_2/2)|m_2) - E(\phi(0)|m_2) - (1-m_2)L_2/2\lambda_2}{\lambda_2}. \tag{A.4}$$

From Eq. (A.1) in the same way we obtain

$$I_1 = \frac{E(\phi(-L_1/2)|m_1) - E(\phi(0)|m_1) - (1-m_1)L_1/2\lambda_1}{\lambda_1}. \tag{A.5}$$

with $m_1 = \cos^2\theta(-L_1/2)$. Finally, substituting integrals (A.4) and (A.5) in Eq. (14) it follows Eq. (15).

A.2. Derivation of Eq. (18)

To calculate Eq. (18) we need to solve the following integrals:

$$I_1 = \int_{-L_1/2}^{0} \sin^2\theta(x)\,\mathrm{d}x, \quad I_2 = \int_{0}^{L_2/2} \sin^2\theta(x)\mathrm{d}x. \tag{A.6}$$

By using $\cos\theta(x) = \sin\phi(x)\cos\theta(-L_1/2)$ Eq. (A.6) becomes

$$I_1 = \frac{L_1}{2} - m_1 I_1^* \tag{A.7}$$

with $m_1 = \cos^2\theta(-L_1/2)$ and

$$I_1^* = \int_{-L_1/2}^{0} \sin^2\phi(x)\,\mathrm{d}x. \tag{A.8}$$

Considering Eq. (9) for $-L_1/2 \leqslant x \leqslant 0$ it follows

$$I_1^* = \int_{-L_1/2}^{0} \mathrm{sn}^2\left(-\frac{x}{\lambda_1} + F(\phi(x)|m_1)\right)\mathrm{d}x. \tag{A.9}$$

After the change of variable $z = -x/\lambda_1 + F(\phi(x)|m_1)$ we obtain

$$I_1^* = \frac{L_1}{2m_1} - \frac{\lambda_1}{m_1}(E(\phi(-L_1/2)|m_1) - E(\phi(0)|m_1)). \tag{A.10}$$

Substituting in Eq. (A.7) we have

$$I_1 = \lambda_1(E(\phi(-L_1/2)|m_1) - E(\phi(0)|m_1)). \tag{A.11}$$

In a similar way for $0 \leqslant x \leqslant L_2/2$ we find

$$I_2 = \frac{L_2}{2} - \lambda_2(E(\phi(L_2/2)|m_2) - E(\phi(0)|m_2)). \tag{A.12}$$

Finally, inserting integrals (A.11) and (A.12) in Eq. (17) we obtain Eq. (18).

References

[1] S.Y. Chou, Proc. IEEE 85 (1997) 652.
[2] C. Chappert, H. Bernas, J. Ferré, V. Kottler, J.-P. Jamet, Y. Chen, E. Cambril, T. Devolder, F. Rousseaux, V. Mathet, H. Launois, Science 280 (1998) 1919.
[3] B.D. Terris, L. Folks, D. Weller, J.E.E. Baglin, A.J. Kellock, H. Rothuizen, P. Vettiger, Appl. Phys. Lett. 75 (1999) 403.
[4] O. Fruchart, M. Klaua, J. Bartel, J. Kirschner, Phys. Rev. Lett. 83 (1999) 2769.
[5] W. Wulfhekel, F. Zavaliche, F. Porrati, H.P. Oepen, J. Kirschner, Europhys. Lett. 49 (2000) 651.
[6] M. Albrecht, T. Furubayashi, M. Przybylski, J. Korecki, U. Gradmann, J. Magn. Magn. Mater. 113 (1992) 207.
[7] J. Hauschild, H.J. Elmers, U. Gradmann, Appl. Phys. Lett. 57 (1998) R677.
[8] S.P. Li, W.S. Lew, J.A.C. Bland, L. Lopez-Diaz, C.A.F. Vaz, M. Natali, Y. Chen, Phys. Rev. Lett. 88 (2002) 087202.
[9] Y. Martin, H.K. Wickramasinghe, Appl. Phys. Lett. 50 (1987) 1455.
[10] K. Koike, K. Hayakawa, Appl. Phys. Lett. 45 (1984) 585.
[11] W. Wulfhekel, J. Kirschner, Appl. Phys. Lett. 75 (1999) 1944.
[12] S. Heinze, M. Bode, A. Kubetzka, O. Pietzsch, X. Nie, S. Blugel, R. Wiesendanger, Science 288 (2000) 1805.
[13] P. Bruno, Phys. Rev. Lett. 83 (1999) 2425.
[14] O. Pietzsch, A. Kubetzka, M. Bode, R. Wiesendanger, Phys. Rev. Lett. 84 (2000) 5212.
[15] J.G. Gay, R. Richter, Phys. Rev. Lett. 56 (1986) 2728.
[16] J. Kohlhepp, U. Gradmann, J. Magn. Magn. Mater. 139 (1995) 347.
[17] J. Lee, G. Lauhoff, J.A.C. Bland, Phys. Rev. B 56 (1997) R5728.
[18] J. Shen, A.K. Swan, J.F. Wendelken, Appl. Phys. Lett. 75 (1999) 2987.
[19] B. Dieny, A. Vedyanev, Europhys. Lett. 25 (1994) 723.
[20] A. Thiaville, A. Fert, J. Magn. Magn. Mater. 113 (1992) 161.
[21] H.J. Elmers, J. Magn. Magn. Mater. 185 (1998) 274.
[22] T. Leineweber, H. Kronmüller, J. Magn. Magn. Mater. 176 (1997) 145.
[23] I.N. Bronstein, K.A. Semendyayev, Handbook of Mathematics, Springer, New York, Berlin, Heidelberg, 1998.
[24] I.S. Gradshteyn, I.M. Ryzhik, Tables of Integrals, Series and Products, Academic Press, New York, 1994.
[25] Xiao Hu, Y. Kawazoe, Phys. Rev. B 49 (1994) 3294.
[26] W.F. Brown, S. Shtrikman, Phys. Rev. 125 (1962) 825.
[27] A. Aharoni, Introduction to the Theory of Ferromagnetism, Oxford University Press, Oxford, 1996.
[28] W.F. Brown, J. Appl. Phys. 39 (1968) 993.
[29] R. Vollmer, Th. Gutjahr-Löser, J. Kirschner, S. van Dijken, B. Poelsema, Phys. Rev. B 60 (1999) 6277.
[30] B. Heinrich, T. Monchesky, R. Urban, J. Magn. Magn. Mater. 236 (2001) 339.
[31] R. Skomski, H.P. Oepen, J. Kirschner, Phys. Rev. B 58 (1998) 3223.